ROMANIAN JOURNAL OF INFORMATION SCIENCE AND TECHNOLOGY
Volume **13**, Number 1, 2010, 49–64

3D Dielectrophoretic Chips: Trapping and Separation of Cell Populations

Ciprian ILIESCU[1], Guillaume TRESSET[2], Liming YU[3], Guolin XU[1]

[1]Institute of Bioengineering and Nanotechnology, Singapore
[2]Laboratoire de Physique des Solides, University of Paris-Sud, CNRS, 91405 Orsay, France
[3]Department of Mechanical and Industrial Engineering, University of Toronto, Ontario, Canada
E-mail: ciliescu@ibn.a-star.edu.sg

Abstract. The paper presents original contributions at manipulation of biological samples using electric field (dielectrophoresis). Design considerations, fabrication processes and experimental results of three original three dimensional (3D) dielectrophoretic (DEP) structures: DEP chip with 3D silicon electrodes, DEP chip with asymmetric electrodes. The paper presents also the experimental results of trapping yeast cells and the methods for separation of two cell populations developed in the above mentioned devices.

1. Introduction

Dielectrophoresis (DEP) is a phenomenon that occurs when a neutral particle is placed in an electric field that is spatially non-homogenous. DEP was first reported by Debye et al in 1954 [1] and further developed by Pohl in the 1970s [2]. The current development of microfabrication techniques for bio-medical applications has resulted in renewed interest in the DEP phenomena especially for applications such as: cell trapping [3] or separation of cell populations [4].

The dielectrophoretic force that generates the movement is strongly dependent on the gradient of the electric field. According to the methods used for achieving this gradient, different solutions were proposed. Travelling wave DEP (Fig. 1a) is the method of changing the phase of the applied electric field [5, 6] in order to achieve the gradient of the electric field between two parallel electrodes. Isolating DEP, the

method presented in Fig. 1b, consists of generating gradient of electric field using of non-homogenous dielectric medium between two parallel-plate electrodes [7, 8]. Chiou *et al* proposed a DEP device where the gradient of the electric field is generated using an optical image on a photodiode surface [9]. Moving DEP, presented in [10] by Kua *et al* is a method where particles, initially trapped using a non-uniform electric field, are moved using a travelling electric field. In the last method, the gradient of the electric field is generated by the non-uniform shape of the electrodes. The electrodes can be thin films [11, 12]– Fig. 1c, 3D pillars [13, 14], 3D electrodes that simultaneously define the microfluidic channel [15] or even a combination between a thin electrode and a 3D electrode [16].

Here we present a study of three different solutions of DEP devices. Their structure, design, fabrication are described and finally the results of yeast cell capturing as well as field-flow methods for separation of two cell populations (live/dead) are presented.

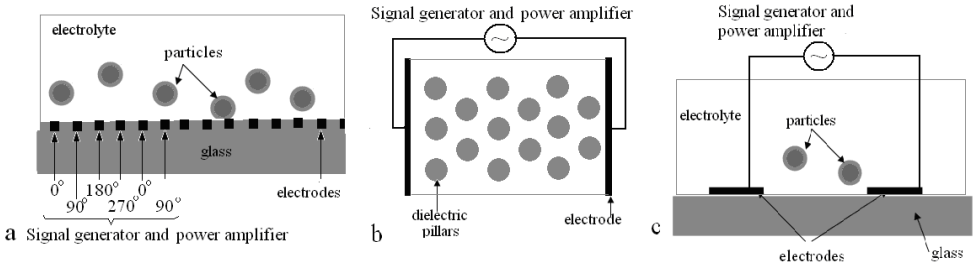

Fig. 1. Schematic representation of DEP devices a) travel wave DEP, b)insulating DEP, c)classical DEP (electrified gradient is generated by the irregular shape of the electrodes).

2. DEP chip with 3D electrodes

2.1. Structure of the device

The DEP device structure, presented in Fig. 2, consists of three main layers: two glass wafers (top and bottom) and an inter-layer of conductive silicon that forms the microfluidic channels and the two DEP electrodes. A metallization layer on the bottom glass surface connects to the bulk silicon electrodes through via holes for easy assembly to a PCB (printed circuit board) Inlet and outlet tubes are glued on the devices for fluid access.

2.2. Theoretical considerations and simulations

To determine the layout of the electrodes, it is necessary to estimate the forces acting on the particle of interest, cells, at different locations within the device. At each point the DEP force must be sufficient to overcome the drag force, which varies with the velocity and is therefore connected to the channel geometry.

If we consider our cells as spherical particles with radius r, placed in an environment with absolute permittivity ε_m, and a applied electric field E with a ∇E field gradient, than the DEP force acting on a particle will be [17]:

$$F = 2\pi r^3 \varepsilon_m R_e[K] \nabla E^2, \tag{1}$$

where $R_e[k]$ is the real part of the polarization factor, defined as:

$$K = \frac{\varepsilon_p - \varepsilon_m}{\varepsilon_p + 2\varepsilon_m}, \quad \varepsilon = \varepsilon - j\frac{\sigma}{\omega}, \tag{2}$$

and ε_p^*, ε_m^* are the complex permittivity of the particle and the medium respectively. The complex permittivity for a dielectric material is defined as its permittivity ε and conductivity σ, at an applied electrical field (E) with an angular frequency of ω. It can be observed that one condition for force generation is that the permittivity of the medium and particle must be different.

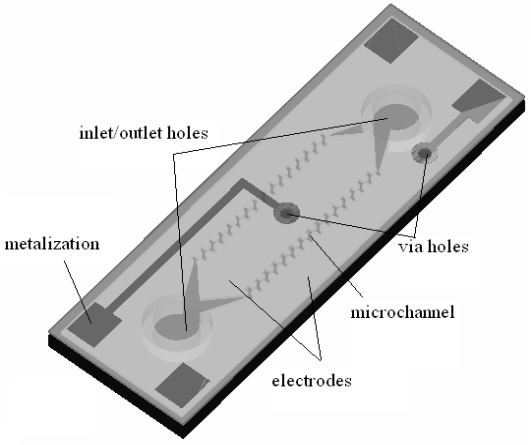

Fig. 2. Schematic view of DEP device with 3D electrodes.

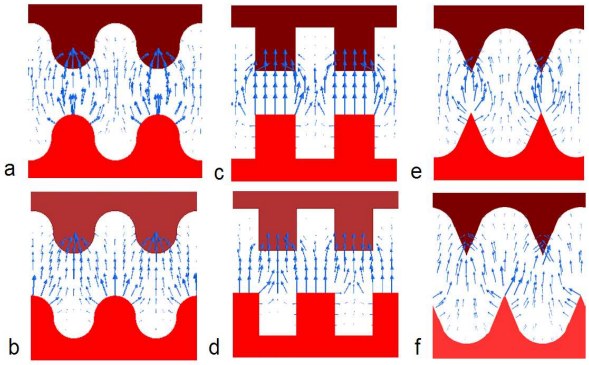

Fig. 3. Configurations of electrode for FEA analysis.

Table 1. Electric field strength and gradient for different electrode configurations with $10V_{pp}$ actuation voltage (the distance between electrodes was 100 μm)

Design	a	b	c	d	e	f
E [$\times 10^4$ V/m]	4.22	4.07	3.68	3.75	8.87	3.61
∇E^2 [$\times 10^5$ V^2/m^3]	2.91	1.76	2.29	2.38	12.8	5.53

To generate the DEP force for cell manipulation an AC voltage with a frequency of 1 kHz – 100 MHz must be applied to the electrodes so that an electric field and its gradient can be generated. From equation (1), the DEP force is proportional to the gradient of the square of electric field, which is determined by the geometry of electrodes and the insulator.

In the DEP device presented the electrode arrangement was developed to maximize the electric field while minimizing the electrical dead volumes such that the DEP force is always sufficient to overcome Stokes' force and concentrate the cells at a relative low actuation voltage, and minimizing fluidic dead volumes. This is a unique requirement for the design described since the electrode geometry also defines the fluidic geometry.

To estimate the electric field generated, triangular, rectangular and semi-circular type electrodes are analyzed using the Maxwell electrostatic finite element analysis (FEA) software. Figure 3 shows examples of electrode configurations. Table 1 lists the maximum electric field and its gradient generated by each electrode configurations. A detail study regarding the gradient of the electric field is presented in [18].

2.3. Fabrication

The main steps of the fabrication process are presented in Fig. 4 and consist of: fabrication of the top glass wafer with inlet/outlet holes (Fig. 4a), first wafer-to-wafer anodic bonding process (Fig. 4b), silicon electrode and microchannel patterning using deep RIE (Figure 4c), assembly of the two glass wafers using a second wafer-to-wafer anodic bonding technique (Fig. 4d), thinning of the glass wafer (Fig. 4e), fabrication of via-holes (Fig. 4f) and metallization leads (Fig. 4g).

A 4″ glass wafer (Pyrex glass Corning 7740) with a thickness of 700 μm was drilled using a diamond bit to create inlet/outlet holes. The holes for inlet/outlet tubing are 1.6 mm in diameter.

A 4″ silicon wafer with <100> crystallographic orientation, p type, heavy doped (conductive) with a resistivity in the range of 0.001 to 0.015 Ωcm, and a thickness of 100 μm, was wafer-to-wafer anodically bonded to a 4″ Pyrex glass wafer (Corning 7740) with a thickness of 500 μm. The bonding process was performed on a EVG wafer bonder. For a good bonding process the wafers were cleaned in piranha (H_2SO_4/H_2O_2 in ratio 2/1) at 120°C for 20 minutes then rinsed in DI water and spin-dried. The bonding process was performed at 305°C, the optimal temperature for bonding of silicon to Corning 7740 (the expansion of silicon and glass at this temperature is similar) [19]. Due to the fact that the fabrication process consisted of two anodic bonding processes, the first anodic bonding was performed at 1000 V, an applied pressure of 1000 mbar, in vacuum, until the value of the current decreased to 40%

of the initial value (4 mA). In this way the bonded glass was conductive at high temperature and a second anodic bonding could be performed. The process resulted in fully bonded wafers without bubbles and un-bonded areas. This was verified visually by the absence of Newton's rings.

The definition of electrodes and microfluidic channels was performed using a deep RIE (Bosch process). For this process a photoresist (AZ9260 from Clariant) mask with a thickness of 5.5 μm was used. The deep RIE etching was done through the silicon wafer with an etch-stop on the glass substrate using SF_6/O_2 for the etching step and C_4F_8 for passivation (Bosch process). A small notching effect was observed in the inlet/outlet regions, at the interface silicon /glass (phenomenon previous described in [20, 21]). This phenomenon was caused by the larger exposed area in this region and the unavoidable non-uniformity of the etching process. The small under-etching in the region of inlet/outlet tube did not affect the performance of the system in our application. Figure 5 shows an SEM picture of the microfabricated silicon electrodes and the channel of the DEP device.

After the removal of the photoresist layer, the wafers were prepared in a similar manner to the first bonding process. The alignment between the glass wafers (with inlet/outlet holes) and the silicon electrodes was performed manually on the bonding frame of a EVG wafer bonder. A misalignment of 0.1–0.3 mm was possible but this was not important for the device fabrication and performance. Alignment on mask aligner equipment requires alignment marks on the glass wafer with drilled holes and this fact makes the fabrication process unnecessarily complicated (another mask and a wet etching process of glass). The second anodic bonding was performed at 450°C, using an applied voltage of 1500 V and 2000 mbarr applied pressure (contact force) in vacuum. The increased temperature was necessary due to the low conductivity of the glass wafers with silicon electrodes. The increased voltage and contact force were applied to increase the electrostatic force and achieve a better contact between the wafers.

For connection of the silicon electrodes via-holes must be formed through the bottom glass wafer. Due to the thickness of glass this process cannot be easily performed. A wet etching process for a 500 μm deep hole from one side is not reported yet in the literature. After a deep wet etching process the size of generated holes becomes very large due to the isotropy of etching (for a 500 μm thick wafer the final diameter is greater than 1 mm). For this reason it was necessary to thin the bottom glass wafer. This process was performed by wet etching in an optimized HF (49%) /HCl (37%) 10/1 solution [22–24]. The glass used – Corning 7740 – was selected not only for its good bonding performance on silicon but also for its low content of oxides that give rise to insoluble products in HF (e.g. CaO, MgO or Al_2O_3). These insoluble products can increase the roughness of the surface due to their re-deposition during the wet etching process. The role of HCl in the solution is to transform the insoluble products into soluble products [25–27]. The presence of insoluble products can drastically reduce the etching rate. The thinning process was performed using a Teflon beaker and slow magnetic stirring until the thickness of the glass was around 100 μm. The uniformity of the process was relatively good with only 20–25 μm thickness variation after 400 μm of etching (the process uniformity was around 5%). The measured

roughness (Ra) of the surface (using an Alpha-step profilometer) was 10 nm. Temporarily bonding a protective silicon wafer with wax assured the protection of the other front side of the processed wafer, during the wet etching.

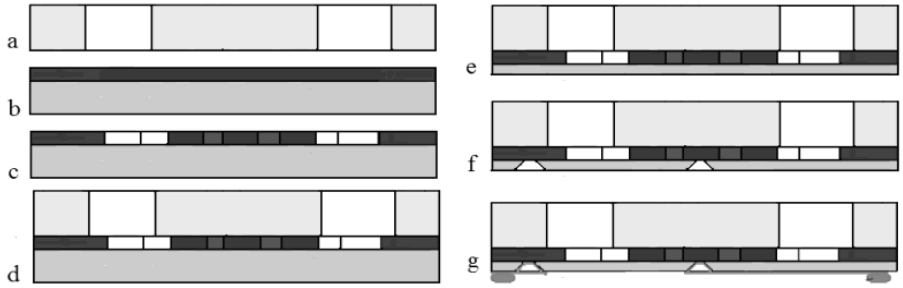

Fig. 4. Main steps of the fabrication process: a) glass wafer, b) first anodic bonding, c) Deep RIE, d) second anodic bonding, e) thinning of glass, f) via holes, g) metallization leads.

A Cr/Au (50 nm/1 μm) masking layer was used for via holes. The patterning of the Cr/Au was performed using 2 μm thick photoresist AZ7220 and classical gold and chromium etchants. The photoresist mask was hard baked at 135°C for 30 minutes in order to improve the adhesion of photoresist on the Au layer. During the etching process the photoresist layer plays an important role. The tensile stress induced in the Cr/Au masking layer [28] can lead to cracks in the mask and the highly concentrated HF solution can penetrate through these cracks and generate pinholes. Although the resistance of photoresist in HF etching solution is poor, the photoresist layer can still improve the overall etching resistance of the masking layer. During the spin-coating process the photoresist penetrates and fills cracks. Hard baking the photoresist increases its adhesion on surfaces and removal of photoresist from the cracks during the wet etching process become more difficult. The thickness of the gold layer also plays an important role in a good etching process. After the wet thinning of the wafer, the surface roughness (R_a) increases from 1 nm up to 10 nm. A large value of surface roughness will increase the number of stress concentration points in the masking layer and therefore increase the number of cracks. By increasing the thickness of the Au layer, the penetration of the etching solution through the cracks (in fact nano-channels) is slower so the overall performance of the masking process is improved. Etching via-holes was performed in the same solution HF/HCl 10/1. No major defects (pinholes and notching defects on the edges) were observed after processing. The Cr/Au mask was removed in the same Cr and Au etchants (the photoresist mask had already pealed off during wet etching in HF/HCl). Another wet etching process of 1.5 minutes (equivalent to a depth etch of 10 μm) was performed mainly to remove the sharpness of the edges and also to remove the non-uniform effects of the wet etching process (during the via-holes etching the etch-stop process cannot be realized due to the small size of the mask and the large depth of etching). The modification of the edge sharpness plays an important role for the subsequent steps of

the fabrication process: the photoresist flow during the spin-coating is more uniform, and the risk of metallization step coverage issues over a sharp edge is eliminated.

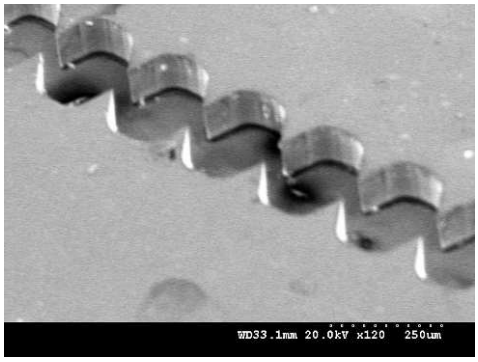

Fig. 5. SEM picture with the fabricated electrodes and microchannel.

The metallization was performed using a Cr/Au (50 nm/1 μm) layer deposited using an e-beam evaporator. A critical step is the patterning of the metal layer due to the extremely non-planar surface of the etched wafer (around 100 μm). The photoresist was deposited using an optimized process described in [29]. After photoresist patterning the Cr/Au layer was etched using a similar process to that used for the Cr/Au etching mask. The fabricated device with inlet/outlet tubes assembled is presented in Fig. 6.

Fig. 6. Photo with DEP chips.

2.4. Cell trapping in a DEP device with 3D electrodes

The testing of the device was performed using yeast cells. 100 mg of yeast, 100 mg of glucose and 2 ml DI water were incubated in an Eppendof tube at 37°C for 2 hours. The cells were then concentrated by centrifugation at 1000 rpm for 1 minute. The supernatant solution was removed and the cell pellet was washed by adding 2 ml of DI water into the tube. The centrifugation and washing process was repeated three

times before the cells were collected and resuspended in the separation buffer, which was a mixture of phosphate buffered saline (PBS) and DI water. The conductivity of the separation buffer was adjusted to about 50 μS/cm using NaCl. The final concentration of the cells was 1×10^7 cell/ml.

A function generator with a sinusoidal wave output was used to generate the drive signal. A linear amplifier was used to amplify the output voltage of the function generator in order to drive the DEP device. The drive signal was increased from 0 to 25 V peak to peak gradually. The signal frequency was anywhere in the range of 20 kHz to 100 kHz. When the actuation signal reached 13 V peak to peak, cells began to move towards the tip of the DEP electrodes, where the electric field gradient was highest. As the actuation voltage increased, the cells moved faster. For a 25 V peak to peak voltage, a stable equilibrium cell concentration pattern was achieved in around 10 seconds. The results of the trapping are presented in Fig. 7.

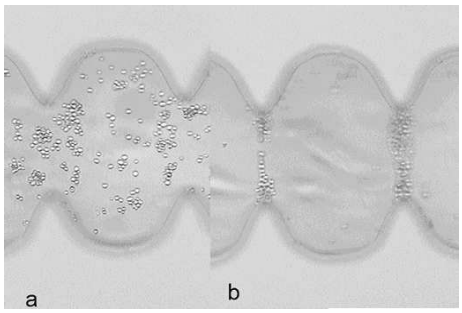

Fig. 7. Optical image with the trapping by positive DEP of yeast cells. (a) Before applying voltage, and (b) after.

The main advantage of the device with 3D electrodes consists of a reduced Joule effect. A detailed analysis regarding Joule effect in different DEP devices is presented in [30, 31].

2.5. Sequential field-flow cell separation method in a DEP chip with 3D electrodes

The method is described in [32] and consists of four steps as illustrated in Fig. 8. First, the microchannel is filled with the mixture of the two populations of particle (Fig. 8a). Second, the particle populations are trapped in different locations of the microfluidic channels (Fig. 8b). The population which exhibits positive dielectrophoresis is trapped in the area where the distance between the electrodes is the minimum whilst the other population that exhibits negative dielectrophoresis is trapped in locations of maximum distance between electrodes. In the next step, increasing the flow in the microchannels will result in an increased hydrodynamic force that sweeps the cell population trapped by positive dielectrophoresis out of the chip (Fig. 8c). In the last step the electric field is removed and the second population is swept out and collected at the outlet (Fig. 8d). The testing was performed with live/dead yeast cells.

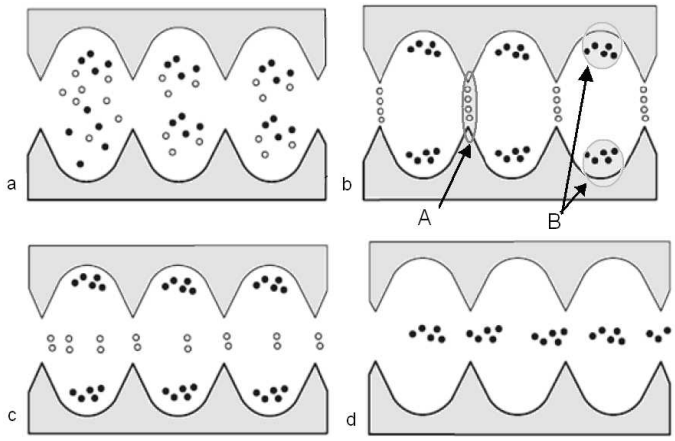

Fig. 8. Main step of the field-flow separation method in a DEP chip with 3D electrodes: a) insertion of the particles in the DEP chip, b) cells separation using positive and negative DEP, c) moving the first population by increasing the velocity of the fluid, d) the second population is released after removing the electric field.

2.6. Continuous field-flow separation of two cell populations in a DEP chip 3D electrodes

The method is a similar with the previous one with the observation that the separation process is performed under continuous flow. The method was presented in detail in [33] and consists of flowing two cell populations (live/dead) through a microfluidic channel, in which the vertical walls are the electrodes of the DEP device.

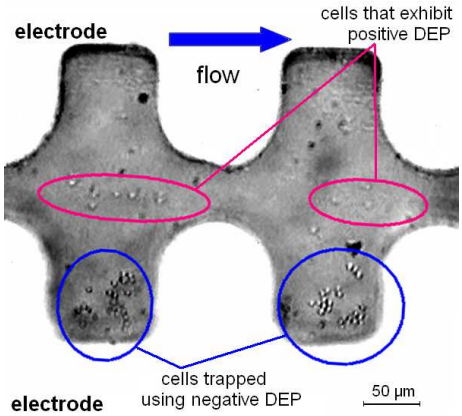

Fig. 9. Optical image of the separation process.

The irregular shape of the electrodes generates both electric field and fluid velocity gradients. As a result, the particles that exhibit negative DEP can be trapped in the

fluidic dead zones, while the particles that experience positive DEP are concentrated in the regions with high velocity and collected at the outlet. The device was tested with dead and living yeast cells. An optical image taken during the separation process is presented in Fig. 9.

2.7. Bidirectional field – flow separation method

For the above presented methods the main disadvantage is the collection of the population trapped in the wells. This disadvantage can be eliminated using a chip with 2 inlets and two outlets, method described in [34]. A schematic drawing as well as an optical image of the device is presented in Fig. 10.

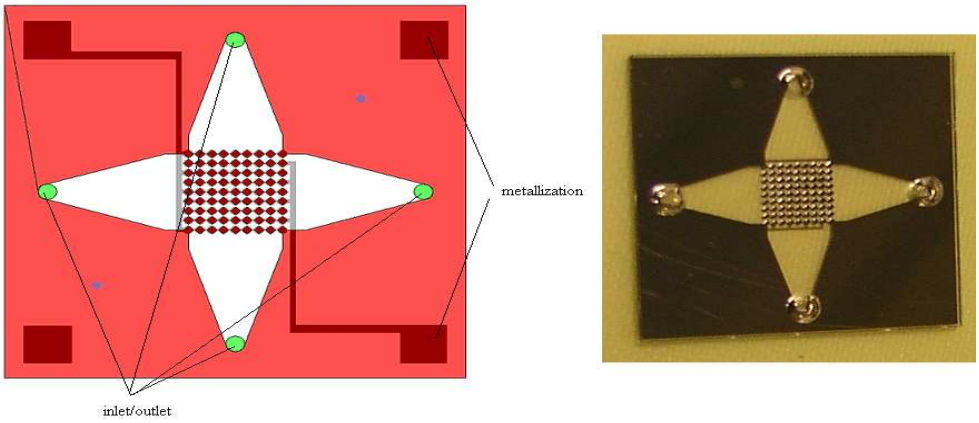

Fig. 10. Schematic drawing and optical image with the device use.

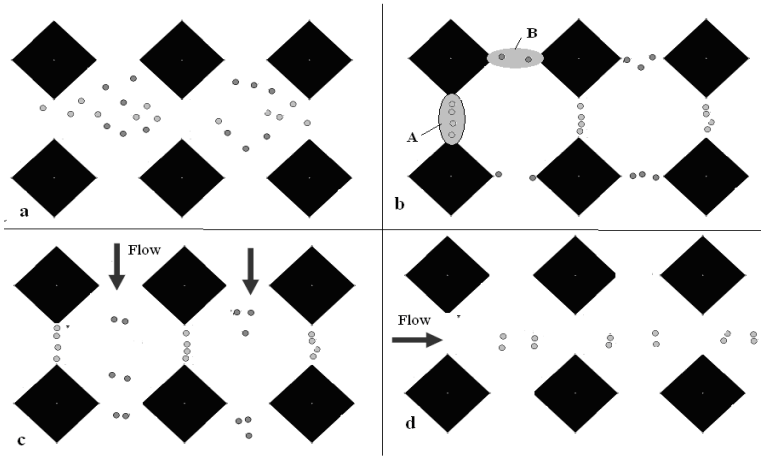

Fig. 11. Bidirectional field-flow separation method: a) insertion of the cell mixture, b) trapping of the cell in different location of the device, c) collection of the first cell population, d) collection of the second population.

The methodology, illustrated in Fig. 11, is as follows: first the solution with the

mixture of two particle population is injected into the microfluidic chamber (Fig. 11a); next the two populations are separated in different locations according to their electrical properties (Fig. 11b); subsequently, one population is collected at one of the outlet by flowing a fresh buffer solution (Fig. 11c) while the other one is collected at the second outlet in the perpendicular direction (Fig. 11d).

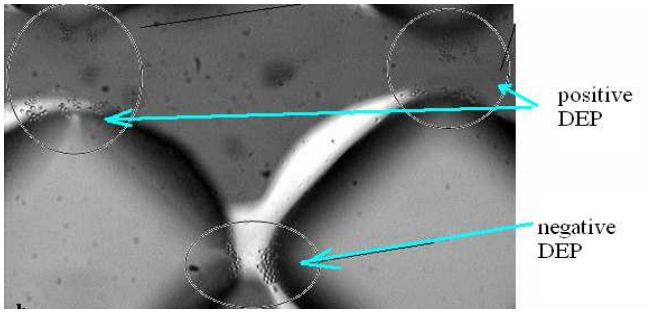

Fig. 12. Optical image taken during the separation process.

Figure 12 presents an optical image taken during the separation process. The two populations are separated using positive and negative DEP on different locations.

3. DEP chip with asymmetric electrodes

3.1. Structure of the DEP chip with asymmetric electrodes

An asymmetric distribution of the electric field in the vertical plane can be possible using a special configuration of the electrodes: a bulk silicon electrode and a thin electrode (Fig. 13).

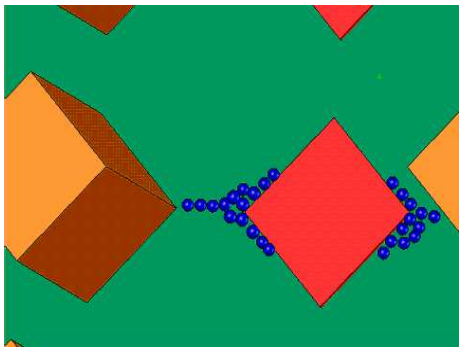

Fig. 13. Structure of the DEP chip with 3D gradient.

The thick electrode defines, at the same time, the walls, while the two glass dies form the ceiling and floor of the microfluidic channel. The top glass die presents two etch-through inlet/outlet holes of the microfluidic channel. In the bottom glass die

isotropic via-holes are performed through the glass for the lead-outs. The proposed DEP structure, with thin and thick electrodes, generates in the vertical plane an asymmetric distribution of the electric field and therefore an enhanced electric field gradient. This aspect is illustrated in Figure 14 where simulations of the electric field for planar and asymmetric DEP structure were performed. As a result, for positive DEP, the particles are trapped near the thin electrode, while for negative DEP the particles are levitated. Compared with typical planar DEP devices, the proposed DEP structure, presents an increased DEP force in the vertical direction.

The fabrication process of the device is presented in detail in [16, 31].

3.2. Analytical considerations and simulation for the DEP structure with asymmetric electrodes

In Figure 15 is presented the variation of DEP force in vertical direction – F_{Z_DEP}) for the planar structure and the structure with asymmetric electrodes. The calculus was performed at the midpoint between the tips, for a yeast cell with a diameter of 5 μm and a relative permittivity of the medium of 81. The graph in Figure 15 shows the variation of F_{Z_DEP} along the vertical direction. It can be noticed that the vertical component of the DEP force – F_{Z_DEP} – is double for the proposed solution in comparison with a typical planar structure. The acute importance of achieving a stronger DEP force in the vertical direction will be demonstrated in the next section.

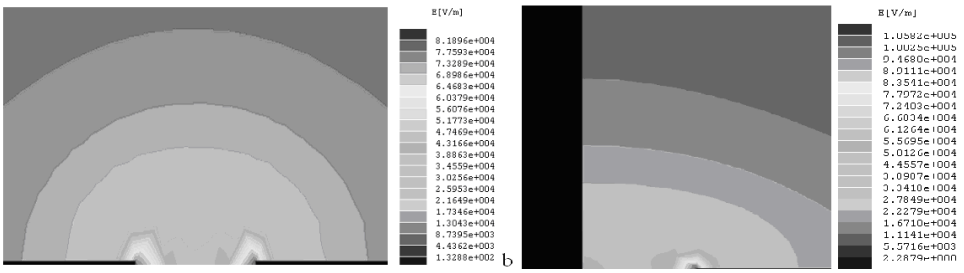

Fig. 14. Maxwell simulations of the electric field in: a) A planar DEP structure, and b) The proposed DEP structure.

In analyzing the effects of F_{Z_DEP}, the buoyancy force (F_B) must also be considered, as both forces act in the same direction. The expression of F_B is well-known:

$$F_B = \frac{4}{3}\pi r^3 \left(\rho_p - \rho_m\right) g \tag{3}$$

where ρ_p and ρ_m are the relative densities of the particle and medium and g is the acceleration due to gravity. For positive DEP, F_{Z_DEP} and F_B act in the same direction, resulting in a faster trapping of the particle on the bottom surface (microchannel floor). Meanwhile, negative DEP provides a F_{Z_DEP} opposite to F_B and enables the generation of an ideal force field because it forces the particles away from the bottom surface of the microfluidic channel by a distance that is related to the manner in which the particle interacts with the electric field. At this distance, F_{Z_DEP} and F_B

are in equilibrium and the total force in vertical direction is zero. This condition can be written as:

$$Re\,[K]\,\nabla E^2 = \frac{2\,(\rho_p - \rho_m)\,g}{3\varepsilon_m} \tag{4}$$

As a result, the particles levitate above the surface according to their physical properties and those of the medium.

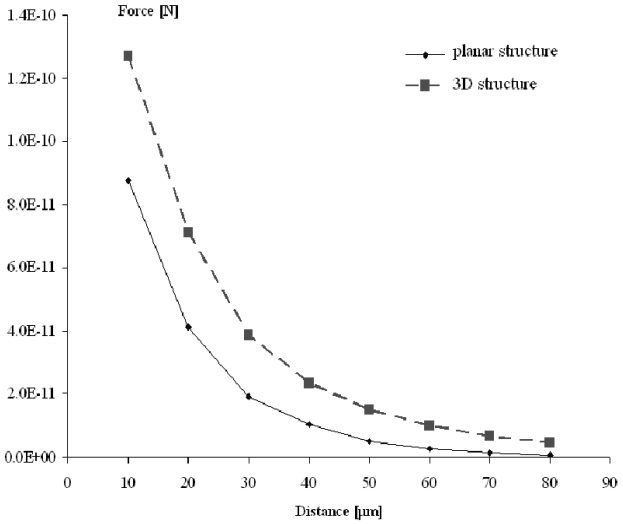

Fig. 15. DEP force versus the distance from the floor of the microfluidic channel along the middle line between the tips of the electrodes for both a typical planar structure and the proposed 3D structure.

3.3 Cell trapping in a DEP device with asymmetric electrodes

The fabrication process of the DEP chip with asymmetric electrodes is similar with previous process described. For the thin electrode a 1 μm-thick amorphous silicon layer (doped with Al) was used. The stress in the layer was measured to be less than 100 MPa compressive. The result of the testing of the DEP device using yeast cell is presented in Fig. 16. The testing setup was performed in similar conditions as the testing of the DEP chip with 3D electrodes.

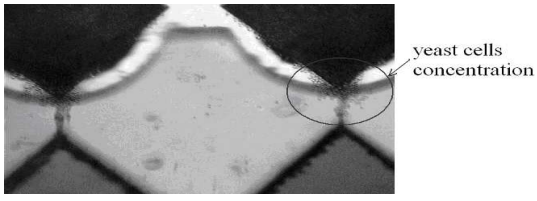

Fig. 16. Yeast cells trapped in the highest electric field regions around thin electrode tips due to positive DEP.

3.4. Continuous field-flow separation method in a DEP device with asymmetric electrodes

Figure 17 illustrates the separation method in a DEP chip with asymmetric electrodes. The mixture with two particle populations is flowed through the microfluidic device. The magnitude of the electric field, its frequency and the medium properties are selected in such a way that one population exhibits positive DEP while the other one negative DEP. Applying the electric field under continuous flow the particles that exhibit negative DEP are levitated due to a strong DEP force in a vertical direction that overcome the buoyancy force while the particles that experience positive DEP are collected on the bottom of the device in the vicinity of the thin electrode. As a result the population that experiences negative DEP will be collected at the outlet. Releasing the electric field and increasing the flow in the microfluidic channel, the second population is collected at the outlet.

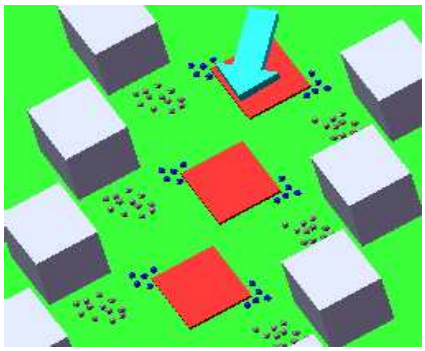

Fig. 17. Schematic view with the separation method: the population that exhibits positive DEP is trapped on the bottom of the device, while the population that experiences negative DEP is levitated and flowed out.

4. Conclusions

The paper presents original structure of DEP devices with 3D electrodes or combinations between 3D and planar electrodes. The main advantages of the structures described are:

- The electrodes define the walls of the microfluidic channel:
- Usage of classical microfabrication techniques;
- Fabrication of the chip at wafer level (chip scale package);
- The devices can work with a small volume of the samples;
- A reduced Joule effect comparing with the DEP device with planar electrodes;

- Due to the reduced Joule effect the devices are suitable for biological applications.

The paper presents also the separation techniques developed in DEP devices with 3D and asymmetric electrodes.

References

[1] DEBYE P., ECKSTEIN B.H., BARBER W.A., ARQUETTE G.J., *Experiments on polymer solution in inhomogeneous electrical fields*, J. Chem. Phys., **22**, 1954, pp. 152–153.

[2] POHL H.A., *Dielectrophoresis*, Cambridge University Press, Cambridge 1978.

[3] HUANG Y., MATHER E.L., BELL J.L., *MEMS-based sample preparation for molecular diagnostics*, Anal. Bioanal. Chem., **372**, 2002, pp. 49–65.

[4] HUGHES M.P., *Strategies for dielectrophoretic separation in laboratory-on-a-chip systems*, Electrophoresis, **23**/16, 2002, pp. 2569–2582.

[5] PETHIGR., TALARY M.S., LEE R.S., *Enhancing travelling-wave dielectrophoresis with signal superposition*, IEEE Eng. Med. Biol. Mag., vol. **22**/6, 2003, pp. 43–50.

[6] CUI L., HOLMES D., MORGAN H., *The dielectrophoretic levitation and separation of latex beads in microchips*, Electrophoresis, vol. **22**, 2001, pp. 3893–3901.

[7] CUMMINGS E.B., SINGH A.K., *Dielectrophoresis in microchips containing arrays of insulating posts: theoretical and experimental results*, Anal. Chem., vol. **75**, 2003, pp. 4724–4731.

[8] ILIESCU C., XU G.L., LOE F.C., ONG P.L., TAY F.E.H., *A 3 dimensional dielectrophoretic filter chip*, Electrophoresis, vol. **28**/7, 2007, pp. 1107–1114.

[9] CHIOU P.Y., OHTA A.T., WU M.C., *Massively parallel manipulation of single cells and microparticles using optical images*, Nature, vol. **436**(21), 2005, pp. 370–372.

[10] KUA C.H., LAM Y.C., RODRIGUEZ I., YANG C., TOUMI K.Y., *Dynamic cell fractionation and transportation using moving dielectrophoresis*, Anal. Chem., vol. **79**, 2007, pp. 6975–6987.

[11] MASUDA S., WASHIZU M., NANBA T., *Novel method for cell fusion in field construction area in fluid integrated circuit*, IEEE Trans. on Ind. Applications, vol. **25**/4, 1989, pp. 732–737.

[12] PARK J., KIM B., CHOI S.K., SU H., LEE S.H., LEE K.I., *An efficient cell separation system using 3D-asymmetric microelectrodes*, Lab Chip, vol. **5**, 2005, pp. 1264–1270.

[13] VOLDMAN J., TONER M., GRAY M.L., SCHMIDT M.A., *Design and analysis of extruded quadrupolar dielectrophoretic traps*, J. Electrostatics, vol. **57**, 2003, pp. 69–90.

[14] PARK B.Y., MADOU M.J., *3-D electrode designs for flow-through dielectrophoretic systems*, Electrophoresis, vol. **26**, 2005, pp. 3745–3757.

[15] ILIESCU C., XU G.L., SAMPER V., TAY F.E.H., *Fabrication of a dielectrophoretic chip with 3D silicon electrodes*, J. Micromech. Microeng., vol. **15**/3, 2005, pp. 494–500.

[16] ILIESCU C., YU L.M., XU G.L., TAY F.E.H., *A dielectrophoretic chip with a 3D electric field gradient*, J. Microelectromech. Syst., vol. **15**/6, 2006, pp. 1506–1513.

[17] JONES T.B., *Electromechanicas of particle*, Cambridge University Press, 1995.

[18] ILIESCU C., TAY F.E.H., XU G.L., YU L., SAMPER V., *A dielectrophoretic chip packaged at wafer level*, Microsystem Technologies, vol. **12**/10–11, 2006, pp. 987–992.

[19] ROGERS T., KOWAL J., *Selection of glass, anodic bonding conditions and material compatibility for silicon-glass capacitive sensors*, Sens. Actuators A, 1995, vol. **46–47**, pp. 113–120.

[20] ILIESCU C., MIAO J., *One mask process for silicon accelerometers on Pyrex glass utilizing notching effect in ICP DRIE*, Electronic Letters, vol. **39**/8, 2003, pp. 658–659.

[21] ILIESCU C., AVRAM M., MIAO J.M., TAY F.E.H., *A new fabrication process for inertial sensors with tunable range*, Rom. Journal of Information Science and Technology, vol. **9**/2, 2006, pp. 83–90.

[22] ILIESCU C., JING J., TAY F.E.H., MIAO J., SUN T.T., *Characterization of masking layers for deep wet etching of glass in an improved* HF/HCl *solution*, Surf.Coat. Techn., vol. **198**/1–3, 2005, pp. 314–318.

[23] ILIESCU C., CHEN B.T., MIAO J.M., *On the wet etching of Pyrex glass*, Sens. Actuators A, vol. **143**/1, 2008, pp. 154–161.

[24] ILIESCU C., *Wet etching of glass for MEMS applications*, Rom. Journal of Information Science and Technology, vol. **9**/4, 2006, pp. 285–310.

[25] ILIESCU C., MIAO J.M., TAY F.E.H., *Optimization of PECVD amorphous silicon process for deep wet etching of Pyrex glass*, Surf. Coat. Techn., vol. **192**/1, 2005, pp. 43–47.

[26] ILIESCU C., TAY F.E.H., MIAO J.M., *Strategies in deep wet etching of Pyrex glass*, Sens. Actuators A, vol. **133**/2, 2007, pp. 395–400.

[27] ILIESCU C., MIAO J.M., TAY F.E.H., *Stress control in masking layers for deep wet micromachining of Pyrex glass*, Sens. Actuators A, vol. **117**/2, 2005, pp. 286–292.

[28] TAY F.E.H., ILIESCU C., JING J., MIAO J.M., *Defect-fre wet etching through Pyrex glass using Cr/Au mask*, Microsystem Technologies, vol. **12**/10–11, 2006, pp. 935–939.

[29] LEE Y.Y., YU L., TAY F.E.H., ILIESCU C., *Characterization of spray coating photoresist for MEMS applications*, Rom. Journal of Information Science and Technology, vol. **8**/4, 2005, pp. 383–391.

[30] TAY F.E.H., YU L., PANG A.J., ILIESCU C., *Electrical and thermal characterization of a dielectrophoretic chip with 3D electrodes for cells manipulation*, Electroch. Acta, vol. **52**/8, 2007, pp. 2862–2868.

[31] ILIESCU C., TRESSET G., XU G.L., *Dielectrophoretic field-flow method for separating particle populations in a chip with asymmetric electrodes*, Biomicrofluidics, vol. **3**/4, 2009, 044104.

[32] YU L., ILIESCU C., XU G., TAY F.E.H., *Sequential field-flow cell separation method in a dielectrophoretic chip with 3D electrodes*, J. Microelectromech. Syst., vol. **16**/5, 2007, pp. 1120–1129.

[33] ILIESCU C., TRESSET G., XU G.L., *Continuous field-flow separation of particle populations in a dielectrophoretic chip with three dimensional electrodes*, Appl. Phys. Lett., vol. **90**/23, 2007, 234104.

[34] ILIESCU C., YU L.M., TAY F.E.H., CHEN B.T., *Bidirectional field flow particle separation method in a dielectrophoretic chip with 3D electrodes*, Sens. Actuators B, vol. **129**/1, 2008, pp. 491–496.